

Information bounds production in replicator systems

Jordi Piñero,^{1,*} Damian R. Sowinski,² Gourab Ghoshal,^{2,3} Adam Frank,² and Artemy Kolchinsky^{1,4,†}

¹ICREA-Complex Systems Lab, Universitat Pompeu Fabra, 08003 Barcelona, Spain

²Department of Physics and Astronomy, University of Rochester, Rochester, NY, 14627, USA

³Department of Computer Science, University of Rochester, Rochester, NY, 14627, USA

⁴Universal Biology Institute, The University of Tokyo, Tokyo 113-0033, Japan

We investigate minimal replicator systems that are able to use information in a functional manner. Specifically, we consider a population of autocatalytic replicators in a flow reactor, subject to fluctuating environments. We derive operational bounds on replicators production in terms of information-theoretic quantities, reflecting contributions from environmental uncertainty, side information, and distribution mismatch. We also derive the optimal strategy, expressed as a function of both intrinsic replicator parameters and environmental statistics. We compare and contrast our findings with existing information-theoretic formalisms such as Kelly gambling. The results are illustrated on a model of real-world self-assembled molecular replicators. For this system, we demonstrate the benefit of internal memory in environments with temporal correlations, and we propose a plausible experimental setup for detecting the signature of functional information. We briefly discuss the role that information processing may play in guiding the evolution of prebiotic replicator networks.

I. INTRODUCTION

Organisms acquire and use information about their environments in order to maintain and propagate themselves. In this sense, living systems are strikingly different from most nonliving systems, which may exhibit statistical correlations with their environments but do not use such correlations for functional purposes. The ability to use information in a functional manner has been termed ‘semantic’ [1–6], ‘meaningful’ [7, 8], or simply ‘functional information’ [9, 10] in the literature. Until now, this ability has been mostly considered in the context of modern organisms, which have sophisticated genetic [8, 11] and sensory [12–15] information-processing systems. Nonetheless, it is possible that functional information appeared early in the origin of life [16], and that it played an important role in facilitating other important transitions in abiogenesis [17, 18].

Here, we investigate a minimal system that can acquire and use information in a functional way. We focus on systems of simple (possibly molecular) replicators in a flow reactor. Molecular replicators have long been studied in the theoretical literature on the origin of life [19–26], and nowadays they are routinely realized in chemical laboratories studying protobiological and synthetic self-replication [27–34]. The replicators are exposed to a fluctuating environment, which may represent either variability across an ensemble of systems or cyclic fluctuations experienced by a single system. Such fluctuations may represent cycles of dry/wet conditions, day/night, seasons, etc. that may have played a key role in the origin of life [35, 36]. We note that similar replicator systems, possibly with cyclic variations, are also studied using modern organisms in microbial ecology [37–41].

Furthermore, we ask whether the relationship between information and function (in our case, replication) can be quantified in an operational manner. To use a classic example from

information theory, recall that Shannon showed that mutual information is the operational quantity that limits the capacity of a noisy channel to transmit messages [42]. In a similar way, we ask whether information about a fluctuating environment can provide operational bounds on functional performance (replication) in a minimal system.

In Sec. III, we introduce our operational measure of interest: the *productivity*, defined as the average rate at which replicators flow out of the reactor during a given interval of time. We then investigate how the productivity depends on the initial concentration of different replicators in the reactor. Our main theoretical results, encapsulated in Eqs. (28)–(34), reveal that productivity has contributions from three information-theoretic terms. At a high level, these terms can be interpreted as (i) a negative contribution due uncertainty about the current state of the fluctuating environment, (ii) a positive contribution due to the benefit derived from a source of side information that helps predict the environment, and (iii) a negative contribution due to the distribution mismatch between the actual initial state of the reactor and the optimal one.

The third mismatch term is the only contribution that depends on the initial proportions of different replicators. We use the term *strategy* to refer to these initial proportions, which may be prepared conditionally on some external variable(s). We derive the expression of the optimal strategy, i.e., the initial proportions that minimize mismatch and thus maximize productivity. The optimal strategy is shown to depend both on intrinsic properties of the replicators (such as their replication rates) and on the statistics of the environmental fluctuations. One rather surprising result of our analysis is that optimal strategies are biased toward slower-growing replicators.

In Sec. IV, we use our formal framework to study a real-world replicator system: the self-assembled photocatalytic replicators developed by Otto and collaborators [43]. As in the original work, we suppose that the system is exposed to active cycles of weak and strong light that favor different replicators. The system also undergoes extended phases of inactivity, during which the replicator concentrations (partially) re-equilibrate due to exchange reactions. The inactive phases allow the system to establish a strategy for exploiting active

* jpinerfe@gmail.com

† artemyk@gmail.com

phases, while possibly maintaining an internal memory. In temporally-correlated environments, we show that this internal memory can serve as a source of side information, leading to an information-theoretic increase in productivity. We verify that our theoretical predictions agree with numerical simulations, assuming relevant parameter regimes.

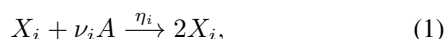
Importantly, our analysis in Sec. IV suggests a plausible experimental setup for detecting the signature of functional information (information leading to increased productivity) in a minimal replicator system. In addition, as we touch upon in the Discussion (Sec. V), it suggests how a replicator network — including both replication and exchange reactions — can behave as a single evolutionary unit and possibly undergo selection for improved information-processing capability.

As we discuss below, our theoretical approach is related to previous work on *substitutional load* and information costs in natural selection [44, 45]. It is also closely related to the seminal work by Kelly on information and multiplicative growth [46]. Kelly’s results, originally operationalized in terms of gambling, have since been used to study the relationship between information, fitness, and phenotypic variability in biology [47–54]. However, there are several important differences between our approach and previous Kelly-type analyses, which allow our results to be directly applied to a broad range of simple chemical and microbial replicator systems. First, our results relate information to productivity in a finite flow reactor, not to unbounded exponential growth, as in existing work. Second, we demonstrate that both ‘betting’ and ‘gambling’ phases of Kelly’s setup can be implemented by a single continuous-time autonomous system. This differs from existing work, where gambling and betting phases are typically separated by discrete pre-programmed life cycle stages. Finally, we demonstrate that a minimal replicator system can implement an internal memory and use it as a source of side information, without any explicit sensory mechanisms.

II. SETUP

We begin by introducing our general physical setup; see also Table I for summary of parameters and variables. We consider a well-mixed continuous-flow reactor with a dilution rate ϕ containing n replicator species X_i indexed by $i \in \{1, \dots, n\}$. Species may represent either biological organisms (e.g., microbes) or abiotic chemical compounds (e.g., self-replicating molecules), though we typically imagine the latter. The reactor is also supplied with reactant species A , a necessary resource for replication, which flows into the reactor at a mass concentration μ .

Each replicator copies itself via an autocatalytic reaction:



where $\nu_i \geq 1$ is the number of reactants required to produce a replicator of species i and $\eta_i \geq 0$ is the replication rate. At time t , we denote the mass concentrations of reactant by $a(t)$ and of replicator species i by $x_i(t)$. We assume that

concentrations evolve according to:

$$\frac{d}{dt}a(t) = \mu\phi - \sum_i \eta_i a(t)x_i(t) - \phi a(t), \quad (2)$$

$$\frac{d}{dt}x_i(t) = (\eta_i a(t) - \phi)x_i(t), \quad \forall i. \quad (3)$$

Note that the stoichiometric coefficients ν_i do not appear in Eqs. (2)-(3). This is because we use mass concentrations throughout, therefore our kinetic equations represent transport of mass, not counts. In addition, the reactions involved in self-replication are typically non-elementary and involve multiple steps. Hence, the equations (2)-(3) are phenomenological, and in particular replication is always assumed to be first-order in reactant concentration $a(t)$. Such kinetics have been observed in chemical replicators [55] and they are consistent with standard models of biological growth (e.g., Monod model) at low reactant concentrations [56, p. 43].

We define two useful quantities: the *total replicator concentration*, $X(t) := \sum_i x_i(t)$, and the *total solute concentration* $S(t) := X(t) + a(t)$. Adding up lines (2)-(3) gives the dynamics of total solute concentration as

$$\frac{d}{dt}S(t) = \phi(\mu - S(t)), \quad (4)$$

which is solved by:

$$S(t) = S(0)e^{-\phi t} + \mu(1 - e^{-\phi t}). \quad (5)$$

Steady-state concentrations are indicated as a^* and x_i^* for the reactant and replicators, and X^* and S^* for the totals. Assuming the generic case with no neutrality (all η_i are different), as well as replication kinetics that are linear in the concentration of a single reactant A , only one replicator can be present in steady state. This result corresponds to the well-known principle of ‘competitive exclusion’ in ecology [57]. If all replicators are present in the initial population, the one remaining replicator in steady state is indicated as

$$r = \underset{i}{\operatorname{argmax}} \eta_i. \quad (6)$$

Here onward, we term the replicator species r as the ‘winner’. The steady-state concentrations are given by

$$a^* = \frac{\phi}{\eta_r} \quad S^* = \mu \quad (7)$$

$$x_r^* = X^* = \mu - \frac{\phi}{\eta_r}, \quad (8)$$

as long as $x_r^* > 0$ (no washout). To avoid washout, we assume that the parameters satisfy $\mu > \phi/\eta_r$.

III. THEORETICAL RESULTS

A. Productivity

Suppose that the chemical system evolves over a time interval $t \in [0, \tau]$ from initial condition $x(0) =$

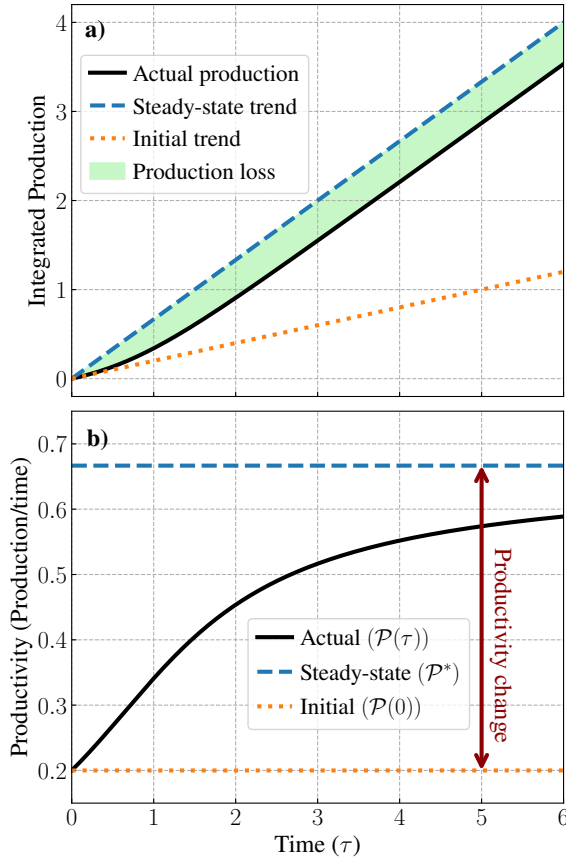


Figure 1. **Productivity patterns.** Result (13) illustrated using a system of two replicators. (a) Total replicators production (in units of mass concentration) integrated over time τ . Shaded green region corresponds to the *production loss* L , as defined in (15). (b) Productivity is production per time. Red arrow indicate productivity change from initial to steady-state values. Parameters: $\eta_1 = 2, \eta_2 = 3, \mu = 1, \phi = 1$; initial concentrations: $a(0) = 0.8\mu, x_1(0) = a(0)/5, x_2(0) = 4a(0)/5$ ($S(0) = S^* = \mu$). For parameter definitions and units, see Table I.

$(x_1(0), \dots, x_n(0)), a(0)$. Our main quantity of interest is *productivity*, defined as:

$$\mathcal{P} := \frac{1}{\tau} \int_0^\tau \phi X(t) dt. \quad (9)$$

Productivity is the time-averaged rate with which replicators flow out of the reactor, having units of mass concentration (mass per volume) per time. In the long-time limit $\tau \rightarrow \infty$, productivity converges to its steady-state value,

$$\mathcal{P}^* := \phi x_r^* = \phi \left(\mu - \frac{\phi}{\eta_r} \right). \quad (10)$$

Note that our assumption that $\mu > a^*$ guarantees that $\mathcal{P}^* > 0$.

To make things concrete, Fig. 1 shows the integrated production and productivity for a simple system with two replicators. In particular, Fig. 1b shows how productivity changes over time as replicator concentrations change, approaching its steady-state value in the long-time limit.

Parameter	Symbol	Units
Inflow concentration of reactant	μ	C
Dilution rate (inverse residence time)	ϕ	T^{-1}
Temporal duration	τ	T
Replication rate of species i	η_i	$C^{-1}T^{-1}$
Variable		
Environment	ε	—
Reactant concentration inside reactor	a	C
Replicator concentration of species i	x_i	C
Total replicator concentration	X	C
Total solute concentration	S	C
Productivity	\mathcal{P}	CT^{-1}
Production loss	L	C
Productivity bound with side information	\mathcal{P}	CT^{-1}
Productivity bound with no side-information	\mathcal{P}_0	CT^{-1}

Table I. Parameters and variables with units: C for mass concentration (mass per volume), T for time. Throughout the text, steady-state values are indicated by a superscript star *. Values of μ, ϕ for environment ε are indicated with subscripts as $\mu_\varepsilon, \phi_\varepsilon$.

In what follows, we study how productivity \mathcal{P} depends on the initial concentrations $\mathbf{x}(0)$ and $a(0)$. To do so, let us consider the winning replicator r . Dividing both sides of (3) by $x_r(t) > 0$ and integrating over $t \in [0, \tau]$ leads to

$$\ln \frac{x_r(\tau)}{x_r(0)} = \eta_r \int_0^\tau a(t) dt - \phi\tau. \quad (11)$$

Recall that $a(t) = S(t) - X(t)$ by definition, so

$$\int_0^\tau a(t) dt = \int_0^\tau S(t) dt - \frac{\tau}{\phi} \mathcal{P}, \quad (12)$$

where we used (9). We integrate using (5) and rearrange to obtain

$$\mathcal{P} = \mathcal{P}^* + \frac{\phi}{\tau \eta_r} \ln \frac{x_r(0)}{x_r(\tau)} + \frac{1 - e^{-\phi\tau}}{\tau} (S(0) - S^*), \quad (13)$$

where \mathcal{P}^* is the steady-state productivity (10).

Expression (13) is our first result. It shows that the productivity, the time-averaged production over a given interval, equals the steady-state productivity plus two correction terms. The first correction term in (13) depends on concentration change of the winner between the initial and final times. This term is negative when the winner's concentration increases, $x_r(\tau) > x_r(0)$, which implies a decrease in productivity (relative to steady-state). This reflects the fact that any replication that increases concentration inside the reactor does not contribute to outflow (i.e., production). Conversely, this first correction term is positive when $x_r(\tau) < x_r(0)$, reflecting excess initial winner concentration that flows out as productivity, without having to be created by replication. In Fig. 1, we provide a simple example for a system with two replicators; in this figure, this first correction term is negative and it leads to the 'delay' between the dashed blue and solid black lines in Fig. 1a.

The second correction term in (13) shows that productivity increases in proportion to the excess initial solute, relative to its steady-state value. To simplify analysis, from this point on, we assume that the initial solute concentration is at its steady-state value:

$$S(0) = S^*, \quad (14)$$

so that the second correction term vanishes. This condition can be achieved by allowing the system to undergo a long transient period prior to $t = 0$, until S reaches steady state. Many of our results below can be generalized beyond assumption (14), at the cost of additional notation.

Result (13) is related to the concept of ‘substitutional load’ in evolutionary biology [44, 58, 59]. Given a biological population with two alleles, substitutional load refers to the cost of replacing the less fit allele with the fitter allele by the process of natural selection. This cost reflects decreased population fitness, i.e., it is proportional to the additional deaths needed to cull the less fit organisms. Kimura showed that the substitutional load can be expressed as the negative logarithm of the initial proportion of the fittest allele [44]. Similarly, the second term in (13) reflects the decrease of productivity associated with the process of increasing the concentration of the winning replicator. Note that Kimura assumed a fixed population size, while we allow the total replicator concentration to vary over time.

We define *production loss* as

$$L := \int_0^\tau \phi (X^* - X(t)) dt, \quad (15)$$

By combining previous results and assuming (14), L can be written explicitly as:

$$L = \frac{\phi}{\eta_r} \ln \frac{x_r(\tau)}{x_r(0)}. \quad (16)$$

In the two-replicator example shown in Fig. 1a, L corresponds to the area between two production curves: the dashed blue line assumes that the reactor is initially filled with the winner, $x_r(0) = X^*$ and for the black straight line we suppose $x_r(0) < X^*$. We can rewrite our expression for productivity (13) as

$$\mathcal{P} = \mathcal{P}^* - \frac{L}{\tau}. \quad (17)$$

Next, we introduce our most important assumption: that the temporal duration τ is long enough so that the system approaches steady state:

$$x_r(\tau) \approx x_r^* = X^*. \quad (18)$$

Given this assumption, the production loss takes the value

$$L^* = \frac{\phi}{\eta_r} \ln \frac{X^*}{x_r(0)}. \quad (19)$$

Combining the above, we reach

$$\mathcal{P} = \mathcal{P}^* - \frac{L^*}{\tau} = \mathcal{P}^* + \frac{\phi}{\tau \eta_r} \ln \frac{x_r(0)}{X^*}. \quad (20)$$

At this point, we introduce the *initial distribution* q as the normalized fraction of concentration (i.e., the proportion of replicator mass) belonging to each replicator species:

$$q_i := \frac{x_i(0)}{X(0)}. \quad (21)$$

Finally, we rewrite (20) as

$$\mathcal{P} = \mathcal{P}^* + \frac{\phi}{\tau \eta_r} \left[\ln q_r + \ln \frac{X(0)}{X^*} \right]. \quad (22)$$

Eq. (22) serves as the basis of much of our analysis below. The meaning of the multiplicative factor $\phi/\tau \eta_r$ is discussed at the end of the following section.

B. Fluctuating environments

We now imagine that our system is placed in a fluctuating *environment*, represented by the discrete random variable E . Each state of the environment, ε , occurs with probability $p_\varepsilon = p(E = \varepsilon)$, and it determines the replication rates $\{\eta_i\}_{i \in \{1, \dots, n\}}$, reflecting the fact that different environments favor different replicator species. From our analysis above, the environment also determines the winning replicator — i.e., the species with the highest replication rate, which we indicate as $r(\varepsilon)$ — as well as the steady-state concentrations a_ε^* and X_ε^* . The environment also determines the dilution rate ϕ_ε and temporal duration τ_ε . The fraction of time spent in environment ε is $p_\varepsilon \tau_\varepsilon / \bar{\tau}$, where we introduce the expected temporal duration

$$\bar{\tau} := \sum_\varepsilon p_\varepsilon \tau_\varepsilon. \quad (23)$$

The choice of environment does not affect the initial concentration vector $\mathbf{x}(0) = (x_1(0), \dots, x_n(0))$. Instead, we suppose that initial concentrations may depend on another discrete random variable Y , which represents the choice of *preparation*. We write the initial concentrations given preparation $Y = y$ as $x_i(0|y)$, and similarly for total concentration, $X(0|y) = \sum_i x_i(0|y)$. For simplicity, we assume that the preparation affects only the initial concentrations, not replication rates (η_i) or reactor parameters (ϕ, μ). As an example, Y may represent different possible experimental preparations in a laboratory setting. More generally, it may represent any external variables (e.g., time of day, physical location of the reactor, etc.) that have an effect on the initial concentrations.

The relative (normalized) initial concentration defines a conditional probability distribution:

$$q_{i|y} := \frac{x_i(0|y)}{X(0|y)}. \quad (24)$$

Here onward, we use the term *strategy* to refer to the conditional distribution q defined in (24). In general, a strategy can be controlled by a number of parameters, which in principle could be tweaked by an experimentalist.

We use $q_{r(\varepsilon)|y}$ to indicate the relative initial concentration assigned to the winner in environment ε given preparation y .

Following (22), under environment ε and preparation y , the productivity is given by:

$$\mathcal{P}_{\varepsilon,y} = \mathcal{P}_{\varepsilon}^* + \frac{\phi_{\varepsilon}}{\tau_{\varepsilon}\eta_{r(\varepsilon)}} \left[\ln q_{r(\varepsilon)|y} + \ln \frac{X(0|y)}{X_{\varepsilon}^*} \right]. \quad (25)$$

In this expression, $\mathcal{P}_{\varepsilon}^* = \phi_{\varepsilon} x_{r(\varepsilon)}^*$ is the steady-state productivity in environment ε , where we applied (10).

Importantly, preparation Y may be correlated with the environment E , and therefore it may serve as a possible source of *side information* about the environment. We suppose that the probability of observing environment ε and preparation y is governed by the joint distribution $p_{\varepsilon,y}$. We then calculate the average productivity (production per time) assuming that environments and preparations are sampled according to $p_{\varepsilon,y}$,

$$\langle \mathcal{P} \rangle = \frac{1}{\bar{\tau}} \sum_{\varepsilon,y} p_{\varepsilon,y} \tau_{\varepsilon} \mathcal{P}_{\varepsilon,y}. \quad (26)$$

Observe that environments are weighted by their temporal duration τ_{ε} , such that long-lived environments contribute more to average production per time $\langle \mathcal{P} \rangle$.

We are interested in how much this expected productivity deviates from the expected steady-state productivity,

$$\langle \mathcal{P}^* \rangle = \frac{1}{\bar{\tau}} \sum_{\varepsilon} p_{\varepsilon} \tau_{\varepsilon} \mathcal{P}_{\varepsilon}^*, \quad (27)$$

which would be reached in the long-time limit ($\tau_{\varepsilon} \rightarrow \infty$ for all environments). This leads to our main result (see Appendix A for details):

$$\langle \mathcal{P} \rangle = \langle \mathcal{P}^* \rangle - \gamma - \Omega C_{\pi,q}(R|Y). \quad (28)$$

In writing (28), we introduce the weighted average log-ratio of total replicator concentrations,

$$\gamma := \frac{1}{\bar{\tau}} \sum_{\varepsilon,y} p_{\varepsilon,y} \frac{\phi_{\varepsilon}}{\eta_{r(\varepsilon)}} \ln \frac{X_{\varepsilon}^*}{X(0|y)}. \quad (29)$$

This constitutes the second contribution to $\langle \mathcal{P} \rangle$ in (28), it can be either positive or negative (depending on the setup). Importantly, it does *not* depend on the initial distribution q . The third term in Eq. (28) depends on the conditional cross-entropy,

$$C_{\pi,q}(R|Y) = - \sum_{r,y} \pi_{r,y} \ln q_{r|y}, \quad (30)$$

where we have introduced the joint distribution $\pi_{r,y}$,

$$\pi_{r,y} := \frac{1}{\Omega \bar{\tau}} \sum_{\varepsilon:r(\varepsilon)=r} p_{\varepsilon,y} \frac{\phi_{\varepsilon}}{\eta_{r(\varepsilon)}}, \quad (31)$$

with the normalization constant

$$\Omega := \frac{1}{\bar{\tau}} \sum_r \sum_{\varepsilon:r(\varepsilon)=r} p_{\varepsilon} \frac{\phi_{\varepsilon}}{\eta_{r(\varepsilon)}}. \quad (32)$$

The distribution π , as will be shown below, specifies the optimal strategy that maximizes productivity.

In some cases, such as our analysis of the real-world replicator system in Sec. IV, it will be convenient to consider periods where the reactor is closed ($\phi = 0$) and therefore there is no production. In such cases, instead of Eq. (26), the productivity should be calculated as

$$\langle \mathcal{P} \rangle := \frac{\alpha}{\bar{\tau}} \sum_{\varepsilon,y} p_{\varepsilon,y} \tau_{\varepsilon} \mathcal{P}_{\varepsilon,y}. \quad (33)$$

where $\alpha \geq 0$ indicates the fraction of time that the reactor is open. All other results derived in this section then follow in the same way, except with $1/\bar{\tau}$ replaced by $\alpha/\bar{\tau}$.

C. Information-theoretic bounds

The cross entropy is a nonnegative cost that can be decomposed into a sum of three information-theoretic contributions:

$$C_{\pi,q}(R|Y) = H_{\pi}(R) - I_{\pi}(R; Y) + D(\pi_{R|Y} \| q_{R|Y}). \quad (34)$$

Let us discuss the three terms in (34) in order. The first is the Shannon entropy of the identity of the winning replicator R under distribution π ,

$$H_{\pi}(R) = - \sum_r \pi_r \ln \pi_r. \quad (35)$$

It quantifies the uncertainty about the winner R in a typical environment. It can be understood as the productivity cost of learning the identity of the winner, in this way eliminating this uncertainty. The second contribution is (minus) the mutual information between the winner R and the preparation Y under distribution π ,

$$I_{\pi}(R; Y) = H_{\pi}(R) - H_{\pi}(R|Y) = \sum_{r,y} \pi_{r,y} \ln \frac{\pi_{r|y}}{\pi_r}. \quad (36)$$

It quantifies the reduction in uncertainty about the winner R provided by the initial preparation Y . It reflects the productivity benefit provided by the ‘side information’, as encoded in the initial preparation. The third term is the Kullback-Leibler (KL) divergence between the actual strategy $q_{R|Y}$ and the conditional distribution $\pi_{R|Y}$,

$$D(\pi_{R|Y} \| q_{R|Y}) = \sum_{r,y} \pi_{r,y} \ln \frac{\pi_{r|y}}{q_{r|y}}. \quad (37)$$

This nonnegative quantity reflects the distribution mismatch between the actual strategy and the optimal strategy specified by π . Due to this mismatch, productivity may be low even when the initial preparation provides a large amount of side information. In simple terms, the system may have information about the environment but not be able to use it in a functional way, i.e., to increase productivity.

Only the third KL term in (34) depends on the initial distribution q , and it reaches its minimum value of zero when the strategy $q_{R|Y}$ matches the distribution $\pi_{R|Y}$. Thus, $\pi_{R|Y}$

represents the strategy that maximizes productivity. However, in a setting where q can only be manipulated by a limited set of control parameters, the optimal strategy π is not always achievable. In Sec. IV, we discuss an example in which π is not achievable.

More generally, using the nonnegativity of KL divergence, we have the bounds on productivity like

$$\langle \mathcal{P} \rangle \leq \mathcal{P} \leq \langle \mathcal{P}^* \rangle - \gamma, \quad (38)$$

where we introduced the information bound \mathcal{P} as

$$\mathcal{P} := \langle \mathcal{P}^* \rangle - \gamma - \Omega [H_\pi(R) - I_\pi(R; Y)]. \quad (39)$$

Eq. (39) is derived directly by substitution of the optimal strategy π into (28). The last inequality in (38) follows from $H_\pi(R) - I_\pi(R; Y) = H_\pi(R|Y) \geq 0$. In absence of preparation Y , the mutual information term in (39) drops out, and Eq. (38) becomes

$$\langle \mathcal{P} \rangle \leq \mathcal{P}_0 \leq \langle \mathcal{P}^* \rangle - \gamma, \quad (40)$$

where the bound \mathcal{P}_0 is defined as

$$\mathcal{P}_0 := \langle \mathcal{P}^* \rangle - \gamma - \Omega H_\pi(R). \quad (41)$$

The last inequality in (40) follows directly from the non-negativity of Shannon entropy.

The fact that the optimal strategy is given by π is similar to the *proportional betting* strategy in Kelly's operational approach to information theory [46, 60]. Similarly, the bounds \mathcal{P} (39) and \mathcal{P}_0 (41) are similar to Kelly's bound on multiplicative growth, with and without side information respectively. The difference between these two upper bounds is proportional to the mutual information,

$$\mathcal{P} - \mathcal{P}_0 = \Omega I_\pi(R; Y). \quad (42)$$

It is worth discussing the optimal strategy π and the normalization constant Ω in a bit more detail. First, observe that Ω (32) multiplies the information terms in Eqs. (22), (39), and (41). To make an analogy to thermodynamics, Ω acts as a kind of 'effective temperature', in that it converts between dimensionless informational quantities (in nats) and productivity (in concentration per time units). To understand its physical meaning, observe that Ω is the average of terms like $\phi_\varepsilon / \bar{\tau} \eta_{r(\varepsilon)}$. For each environment ε , the dilution rate ϕ_ε determines how fast concentrations within the reactor flow out as productivity. The denominator $\bar{\tau} \eta_{r(\varepsilon)}$ is proportional to the number of doublings of the fittest replicator during average duration $\bar{\tau}$. Thus, the cost/benefit of information is greater when dilution rates are high, but also when winning replicators are slow (fewer doublings). This arises from the fact that slower replicators are less able to recover from sub-optimal initial conditions.

Similarly, the optimal strategy $\pi_{r,y}$ (31) is biased towards replicators that undergo higher dilution rates (larger ϕ_ε) and are slower (smaller $\eta_{r(\varepsilon)}$), relative to the actual distribution of winners and preparations. This bias may appear counter-intuitive, but it can be understood using the argument mentioned in the last paragraph: a slower winner is less able to recover from a low initial concentration, thus it incurs a greater productivity loss.

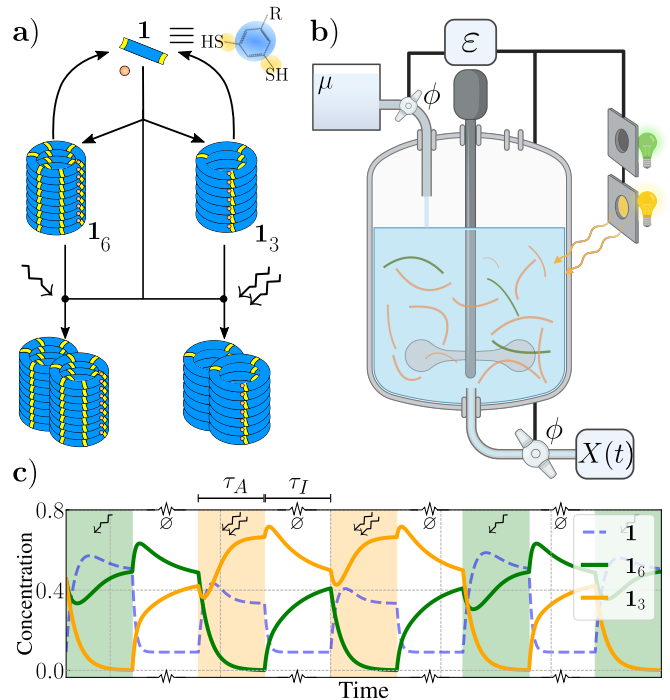


Figure 2. **Photocatalytic replicator system** [43]. (a) Schematic of simplified reaction network. ζ indicates replication under weak light environment, $\zeta\zeta$ indicates replication reaction under strong light environment (see also Table II). (b) Experimental setup, including flow reactor fed by reservoir of monomers 1 at concentration μ . During active phases (weak ζ or strong $\zeta\zeta$ light environments), the reservoir feeds the reactor with rate ϕ . During inactive phase (\emptyset), light is switched off and the flow is stopped, allowing the system to establish a 'bet' for the next active environment. Productivity \mathcal{P} is quantified by measuring replicator concentration $X(t)$ at the outlet. (c) Typical concentration trajectories for monomer 1 and two replicators (1_6 and 1_3), given cycles of inactive phases (white regions of length τ_I) and randomly-chosen active environments (shaded regions of length τ_A); timescale of inactive phase is longer but rescaled for illustrative purposes. Parameters $\{\eta_1, \eta_2, \mu\}$ same as in Fig. 1, $\phi_\zeta = \phi_{\zeta\zeta} = \phi = 1$, $\phi_\emptyset = 0$, $\tau_A = 6$, $\tau_I = 10^5$, $b = 0.5$, $\lambda = 2$ and $k_f/k_d = 10$. For parameter definitions and units, see Table II.

IV. APPLICATION TO A REAL-WORLD SYSTEM

In this section, we propose a potential experiment that relates our information-theoretic findings to empirically measurable quantities. Drawing inspiration from recent work in prebiotic chemistry [43, 61], we study photocatalytic molecular self-replicators in a flow reactor. By considering this system, we verify our information-theoretic bounds, while also showing that this autonomous system can implement a strategy and maintain an internal memory that provides a source of side information.

A. System and fluctuating environment

In Ref. [43], the authors demonstrated two self-replicating species of complex synthetic molecules (termed 1_6 and 1_3)

representing hexameric and trimeric macrocycles that self-assemble from a monomer species (termed $\mathbf{1}$). These macrocycles spontaneously stack to form respective fibers that catalyze their own production. Furthermore, by binding these replicators to photosensitive co-factors, the authors showed that these fibers enhance self-replication in response to different light stimuli. Under the right chemical conditions, replicator $\mathbf{1}_6$ wins in a *weakly lit* environment, and $\mathbf{1}_3$ wins in a *strongly lit* one. Autocatalysis does not occur when the system is placed in *dark* conditions. In addition to autocatalysis, formation and degradation reactions exchange matter between polymers and monomer. We assume that such ‘exchange reactions’ occur at slow rates at all times. For details, see Fig. 2a and Table II.

We model this system as $n = 2$ replicator species in a well-mixed reactor. We indicate the mass concentrations of $\mathbf{1}$, $\mathbf{1}_6$ and $\mathbf{1}_3$ as a , x_1 , x_2 , respectively, and use $X = x_1 + x_2$ to indicate the total concentration of replicators. The reactor is coupled to an external cycle that turns light and flow *on* and *off*, which we denote as *active* and *inactive* phases, respectively. Each active phase has duration τ_A . During this time, the reactor is coupled to a reservoir containing reactant $\mathbf{1}$ at concentration μ , while inflow/outflow occurs with dilution rate ϕ . In addition, the system is exposed to an environment with either *weak light* (indicated as \mathcal{L}), which favors replicator $\mathbf{1}_6$, or *strong light* (indicated as \mathcal{L}'), which favors replicator $\mathbf{1}_3$. Each active phase is followed by an inactive phase of duration τ_I (indicated as \emptyset). During this time, flow is turned off, the system is kept in the dark, and only exchange reactions occur.

This basic setup is illustrated in Fig. 2b. The dynamics of the reactant and two replicators during the active and inactive phases are described in more detail below, and are shown for illustration in Fig. 2c.

Importantly, the weak \mathcal{L} or strong \mathcal{L}' environments can exhibit temporal correlations. For simplicity, we assume that the stochastic process over environments is stationary and first-order Markovian, and we use $p_{\varepsilon|\varepsilon_-}$ to indicate the conditional probability that a previous environment $\varepsilon_- \in \{\mathcal{L}, \mathcal{L}'\}$ is followed by the next environment $\varepsilon \in \{\mathcal{L}, \mathcal{L}'\}$ (always with an inactive phase in between). We use p_ε to indicate the steady-state distribution of this Markov chain, and $p_{\varepsilon, \varepsilon_-} := p_{\varepsilon|\varepsilon_-} p_{\varepsilon_-}$ to indicate the steady-state joint probability of environment $\varepsilon_- \in \{\mathcal{L}, \mathcal{L}'\}$ followed by environment $\varepsilon \in \{\mathcal{L}, \mathcal{L}'\}$.

The environment random variable E has two outcomes $\{\mathcal{L}, \mathcal{L}'\}$ which occur with probability $(p_{\mathcal{L}}, p_{\mathcal{L}'})$. Note that the inactive phase is not treated as an environment since it does not contribute to outflow. Also, as we will see below, the environment during the previous active phase may influence the initial condition of the current active phase. For this reason, the previous environment $\varepsilon_- \in \{\mathcal{L}, \mathcal{L}'\}$ can serve as a source of side information Y . For notational convenience, we use the random variable $E_- \equiv Y$ to refer to the previous active environment. It has two outcomes $\{\mathcal{L}, \mathcal{L}'\}$, which co-occur with the environment E of the current active phase according to the joint probability $p_{\varepsilon, \varepsilon_-}$.

We will consider environments with different kinds of temporal correlations between ε and ε_- , as quantified by the sign of coefficient (see Appendix B 3)

$$p_{\mathcal{L}, \mathcal{L}} - p_{\mathcal{L}} p_{\mathcal{L}} = p_{\mathcal{L}', \mathcal{L}'} - p_{\mathcal{L}'} p_{\mathcal{L}'} \quad (43)$$

Parameter	Symbol	Units
Duration of active phases (active time)	τ_A	T
Duration of inactive phases (inactive time)	τ_I	T
Dimensionless inactive timescale ($\lambda = k_d \tau_I$)	λ	1
Bias in favor of formation of $\mathbf{1}_6$	b	1
Formation rate of $\mathbf{1}_6$ ($k_1 = k_f b$)	k_1	T ⁻¹
Formation rate of $\mathbf{1}_3$ ($k_2 = k_f(1 - b)$)	k_2	T ⁻¹
Degradation rate of $\mathbf{1}_6$ and $\mathbf{1}_3$	k_d	T ⁻¹

Exchange	Weak light (\mathcal{L})	Strong light (\mathcal{L}')
$\mathbf{1} \xrightleftharpoons[k_d]{k_1} \mathbf{1}_6$	$\mathbf{1} + \mathbf{1}_6 \xrightarrow{\eta_1} \mathbf{1}_6 + \mathbf{1}_6$	$\mathbf{1} + \mathbf{1}_3 \xrightarrow{\eta_2} \mathbf{1}_3 + \mathbf{1}_3$
$\mathbf{1} \xrightleftharpoons[k_d]{k_2} \mathbf{1}_3$	$\emptyset \xrightarrow{\mu\phi} \mathbf{1}$ and $\mathbf{1}, \mathbf{1}_6, \mathbf{1}_3 \xrightarrow{\phi} \emptyset$	

Table II. *Top*: Parameters used for model of photocatalytic replicators. T for units of time. *Bottom*: Simplified reaction network for replicating macrocycles $\mathbf{1}_6$ and $\mathbf{1}_3$, which self-assemble from monomers $\mathbf{1}$. Active environments with weak (\mathcal{L}) or strong (\mathcal{L}') light conditions lead to self-replication of $\mathbf{1}_6$ or $\mathbf{1}_3$, respectively. During the inactive phase, only exchange reactions take place.

We say that the environments are (positively) *correlated* when this coefficient is strictly positive,

$$p_{\mathcal{L}, \mathcal{L}} - p_{\mathcal{L}} p_{\mathcal{L}} > 0. \quad (44)$$

We say that the environments are *uncorrelated* when the coefficient (43) is equal to zero and *anticorrelated* when it is strictly negative. In simple terms, the active condition (weak or strong) tends to repeat in correlated environments, and alternate in anticorrelated environments.

The production of replicators is tracked by measuring the outflow of both $\mathbf{1}_6$ and $\mathbf{1}_3$ at the outlet of the reactor. Since the reactor remains closed during inactivity, only active phases contribute to productivity. However, inactive phases allow the system to (partially) reset its state, thus setting up the initial condition for the subsequent active phase. As we will see below, the parameters of the exchange reactions (which still occur during inactive phases) affect the initial conditions of the subsequent active phase, thus also the ‘strategy’ that determines the system’s productivity. We will classify the best possible strategies depending on whether the environments are correlated or anticorrelated.

Borrowing terminology from Kelly original work [46]: our inactive phase is interpreted as placing a ‘bet’, in which the system autonomously sets a strategy by preparing the initial condition for the next active round. Our active phase is akin to the ‘gambling’ phase, in which the system evolves towards the steady state dominated by the corresponding winner in the environment (light) state.

B. Reactions and dynamics

We describe the chemical reaction network introduced in [43] by a coarse-grained set of reactions summarized in Table II. Our system involves spontaneous formation and degra-

degradation reactions (left column in Table II), which effectively re-balance the concentrations of the two replicators and the monomer. Here, we assume both replicators have the same degradation rate, k_d . Spontaneous formation occurs at different rates, k_1 and k_2 , for replicators $\mathbf{1}_6$ and $\mathbf{1}_3$, respectively. We define $k_f := k_1 + k_2$ and reparameterize k_1 and k_2 by introducing a *bias* $b \in [0, 1]$ such that

$$k_1 = bk_f \quad \text{and} \quad k_2 = (1 - b)k_f, \quad (45)$$

For simplicity, we assume that the system can be set to favor spontaneous formation against degradation ($k_f \gg k_d$), although this assumption can be generalized. To allow the slow formation and degradation reactions to reset concentrations during the inactive phase, we usually assume that the inactive timescale is longer than the active one ($\tau_I \gg \tau_A$). This can be imagined as periodic bursts of activity followed by long relaxation (inactive) periods. It is useful to characterize the inactive phase by a *dimensionless inactive timescale*, defined as:

$$\lambda := k_d \tau_I. \quad (46)$$

In simple terms, λ is the number of degradation events during the inactive phase per replicator.

During activity, we account for selective photocatalysis by letting the respective replication rates be

$$\eta_{1,\varepsilon} = \eta_1 \delta_{\varepsilon, \mathcal{L}} \quad \text{and} \quad \eta_{2,\varepsilon} = \eta_2 \delta_{\varepsilon, \mathcal{L}'}, \quad (47)$$

with constants $\eta_1 > 0$ and $\eta_2 > 0$. This indicates that $\mathbf{1}_6$ replicates only under environment $\varepsilon = \mathcal{L}$ and $\mathbf{1}_3$ only under environment $\varepsilon = \mathcal{L}'$. Note that in our example, the winning replicators (R) and the environments (E) are in a one-to-one relation, the two random variables are equivalent, $R \equiv E$.

We study trajectories in active and inactive phases in Appendices B 1 and B 2. We assume τ_A is long enough so that the system reaches steady state within each active phase. This assumption implies that, at the end of any active phase, all the remaining dependence on the previous history is erased. The proceeding inactive phase will therefore depend only on the previous environment $\varepsilon_- \in \{\mathcal{L}, \mathcal{L}'\}$.

In Appendix B 2, we derive analytical expressions for the replicator concentrations at the end of an inactive phase as functions of b and λ and conditioned on the previous environment. These concentrations serve as the initial condition of the subsequent active phase, and their relative proportions determine the strategy q , see Eq. (24). As discussed above, here ε_- enters in q as a variable that contains side information about the environmental fluctuations. In other words, the strategy is characterized by $q_{R|E_-}$, which is also a function of $\{b, \lambda\}$.

The connection between the strategy and side information ε_- can also be interpreted as an intrinsic *first-order memory* of the system. The memory is first-order because it only depends on the last environment, since it is reset by the end of every active phase (for a visual example, see Fig. 2c). As discussed below, under positive temporal correlations between consecutive environments, such a memory mechanism can be exploited to increase productivity. In the limit of $\lambda \rightarrow \infty$,

steady state is reached within every inactive phase. In this case, internal memory of ε_- is effectively reset during each inactive phase, and can no longer be exploited. In this case, the strategy q_R does not utilize any side information.

C. Productivity and information

We now calculate the average productivity for the photocatalytic replicator system. Recall from the last subsection that, due to incomplete relaxation during the inactive phase, the identity of the previous environment $\varepsilon_- \in \{\mathcal{L}, \mathcal{L}'\}$ can serve as side information for the current environment $\varepsilon \in \{\mathcal{L}, \mathcal{L}'\}$. We then compute the average productivity as

$$\langle \mathcal{P} \rangle = \frac{\tau_A}{T} \sum_{\varepsilon, \varepsilon_-} p_{\varepsilon, \varepsilon_-} \mathcal{P}_{\varepsilon, \varepsilon_-}. \quad (48)$$

Here we used Eq. (33) along with $\bar{\tau} = \tau_A$ and $\alpha = \tau_A/T$ (the fraction of time the reactor is in the active phase and open).

Following the expressions given in (28), (34) and (31)-(32), for this setup we have:

$$\langle \mathcal{P} \rangle = \langle \mathcal{P}^* \rangle - \gamma - \Omega C_{\pi, q}(R|E_-). \quad (49)$$

Here, the steady-state productivity is given by:

$$\langle \mathcal{P}^* \rangle = \frac{\tau_A}{T} (p_{\mathcal{L}} \mathcal{P}_{\mathcal{L}}^* + p_{\mathcal{L}'} \mathcal{P}_{\mathcal{L}'}^*), \quad (50)$$

where $\mathcal{P}_{\varepsilon}^*$ are obtained by following the procedure discussed in Appendix B 1. Moreover, we also have the terms

$$C_{\pi, q}(R|E_-) = H_{\pi}(R) - I_{\pi}(R; E_-) + D(\pi_{R|E_-} \| q_{R|E_-})$$

$$\gamma = \frac{\phi}{T} \sum_{\varepsilon, \varepsilon_-} \frac{p_{\varepsilon, \varepsilon_-}}{\eta_{\varepsilon}} \ln \frac{X_{\varepsilon}^*}{X_{\mathcal{O}|\varepsilon_-}(\lambda)}. \quad (51)$$

Here, $X_{\mathcal{O}|\varepsilon_-}(\lambda) = X(0|y)$ indicates the total concentration at the end of the inactive phase, which depends on the preceding environment ε_- (the side information). An analytical expression for $X_{\mathcal{O}|\varepsilon_-}(\lambda)$ is given in Appendix B 2. Following (31), but with $1/\bar{\tau}$ replaced by $\alpha/\bar{\tau} = 1/T$, we derive our optimal distribution π as

$$\pi_{1, \varepsilon_-} = \frac{\phi}{\Omega T} \frac{p_{\mathcal{L}, \varepsilon_-}}{\eta_1}, \quad \pi_{2, \varepsilon_-} = \frac{\phi}{\Omega T} \frac{p_{\mathcal{L}', \varepsilon_-}}{\eta_2}, \quad (52)$$

for $y = \varepsilon_- \in \{\mathcal{L}, \mathcal{L}'\}$ and normalization constant

$$\Omega = \frac{\phi}{T} \left(\frac{p_{\mathcal{L}}}{\eta_1} + \frac{p_{\mathcal{L}'}}{\eta_2} \right). \quad (53)$$

D. Maximizing productivity

As shown in Eq. (39), productivity is maximized when the strategy $q_{R|E_-}$ matches the distribution $\pi_{R|E_-}$, at which point $\langle \mathcal{P} \rangle = \mathcal{P}$. However, it turns out that one cannot always make $q_{R|E_-}$ equal to $\pi_{R|E_-}$ simply by varying the control parameters chosen for this numerical experiment, namely $\{b, \lambda\}$.

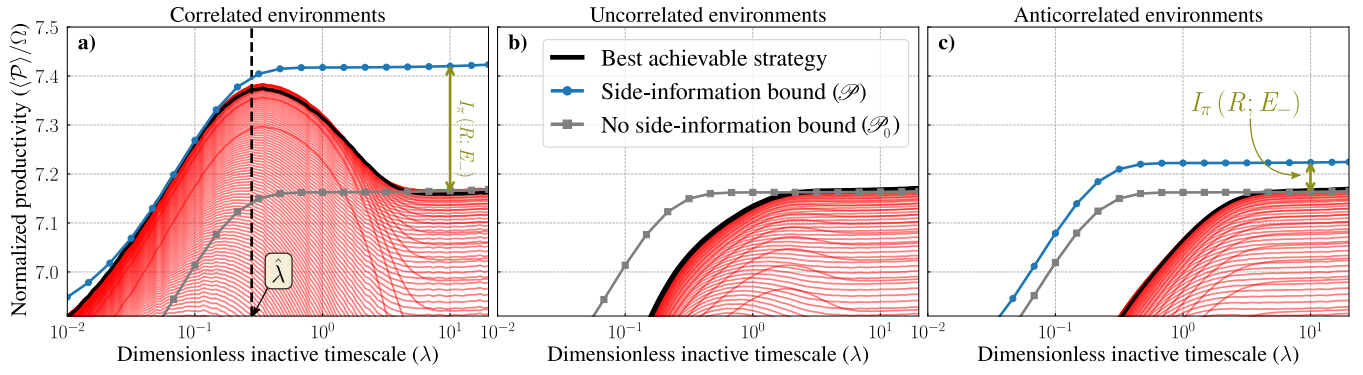


Figure 3. **Information and productivity in photocatalytic replicator system.** Numerical results showing normalized average productivity, $\langle \mathcal{P} \rangle / \Omega$ for two control parameters: $\lambda := k_d \tau_I$ (dimensionless inactive timescale) shown on horizontal axis, b (bias for spontaneous formation of replicator $\mathbf{1}_6$) shown as different red lines (other parameters same as in Fig. 2c). Black lines indicate productivity computed using \hat{b} (54) in (a), and $\hat{b}_{\lambda \rightarrow \infty}$ (55) in (b) and (c). Blue line indicates productivity bounds \mathcal{P} (39) with side information (about previous environment E_-); gray line indicates productivity bound \mathcal{P}_0 (41) without side information. Subplots (a), (b) and (c) correspond to temporally correlated, uncorrelated and anticorrelated environments, respectively. For correlated environments, the best achievable strategy has a finite timescale $\hat{\lambda}$ (54). Subplot (a) verifies bound (42), which shows that increase of maximum productivity is proportional to mutual information provided by side information.

Nonetheless, we can approximately solve for the *best achievable strategy* given our set of controls. To do so, we explore how productivity varies with formation bias b and inactive timescale λ ; we assume fixed values for $\{\mu, \phi, \tau_A, \tau_I, \eta_1, \eta_2\}$ (see Tables I-II for reference).

There are two different ways of varying λ . For instance, one could keep degradation rate k_d fixed and change τ_I , the duration of the inactive phase. However, this affects the value of the cycle period T and thus the average productivity (48). In our example, we vary λ by rescaling the overall formation and degradation rates $\{k_f, k_d\}$, while keeping τ_I fixed. In practice, this could be accomplished by changing the temperature of the reactor, adding catalysts, etc.

In Appendix B 4, we derive the best achievable strategy by expressing $q_{R|E}$ as a function of $\{b, \lambda\}$, and then finding the values that minimize $C_{\pi, q}(R|Y)$. It turns out that the best achievable strategy depends on whether the environments are correlated, uncorrelated, or anticorrelated. Results for temporally correlated, uncorrelated, and anticorrelated environments are shown in Fig. 3a, Fig. 3b and Fig. 3c (respectively).

In particular, for correlated environments (44), the best achievable strategy has bias and inactive timescale

$$\hat{b} \approx \frac{\pi_{1|_{\mathcal{E}\mathcal{E}}}}{\pi_{1|_{\mathcal{E}\mathcal{E}}} + \pi_{2|_{\mathcal{E}\mathcal{E}}}} \quad \hat{\lambda} \approx -\ln(1 - \pi_{1|_{\mathcal{E}\mathcal{E}}} - \pi_{2|_{\mathcal{E}\mathcal{E}}}). \quad (54)$$

In Appendix B 3, we also show that $\pi_{1|_{\mathcal{E}\mathcal{E}}} + \pi_{2|_{\mathcal{E}\mathcal{E}}} < 1$, so $\hat{\lambda}$ is well-defined. Under this strategy, productivity approaches the side information bound \mathcal{P} (39).

For uncorrelated and anticorrelated systems, where inequality (44) does not hold, the inactive timescale diverges as $\hat{\lambda} \rightarrow \infty$. In essence, memory decreases productivity in uncorrelated and anticorrelated environments, thus the best strategy is to have long inactive periods where all memory is erased. This effect is related to the fact that a bit flip cannot be implemented by a two-state Markov chain [62]: in our case, the two

replicators represent the two states of the bit, and the Markov chain is captured by the linear exchange reaction that take place during the inactive phase (see Table II).

In the limit $\hat{\lambda} \rightarrow \infty$, the best bias is given by the marginal probability:

$$\hat{b}_{\lambda \rightarrow \infty} = \pi_{1, \mathcal{E}} + \pi_{1, \mathcal{E}\mathcal{E}} = \pi_1. \quad (55)$$

In this case, productivity under the best achievable strategy approaches the no-side-information upper bound \mathcal{P}_0 (41).

In Fig. 3, we show numerical results for normalized productivity $\langle \mathcal{P} \rangle / \Omega$ (in dimensionless units) against the inactive timescale λ . Different lines show reactors with different bias values b . To explore correlated, uncorrelated, and anticorrelated environments, we generate environments using a Markovian process with different transition probabilities between consecutive environments. The subplots show $p_{\mathcal{E}|\mathcal{E}} = .95, p_{\mathcal{E}\mathcal{E}|\mathcal{E}\mathcal{E}} = .85$ (correlated, Fig. 3a), $p_{\mathcal{E}|\mathcal{E}} = p_{\mathcal{E}\mathcal{E}|\mathcal{E}\mathcal{E}} = .75, p_{\mathcal{E}\mathcal{E}|\mathcal{E}\mathcal{E}} = p_{\mathcal{E}\mathcal{E}} = .25$ (uncorrelated, Fig. 3b), and $p_{\mathcal{E}|\mathcal{E}} = .67, p_{\mathcal{E}\mathcal{E}|\mathcal{E}\mathcal{E}} = .005$ (anticorrelated, Fig. 3c). Marginals $p_{\mathcal{E}} = p_{\mathcal{E}\mathcal{E}} = 1 - p_{\mathcal{E}\mathcal{E}\mathcal{E}} = .75$ are equal in Fig. 3a-c. Numerical productivity values are computed by running the system for 5×10^6 cycles.

In Fig. 3, we see that maximum productivity is closely achieved by the best strategies predicted by Eqs. (54) and (55) (black lines). For both correlated and anticorrelated environments (Fig. 3a,c), productivity is bounded by the side-information bound \mathcal{P} (blue line), while in uncorrelated environments (Fig. 3b), productivity is bound by the no side-information bound \mathcal{P}_0 (gray line). Moreover, in correlated environments, Fig. 3a, productivity exceeds \mathcal{P}_0 at intermediate λ values, moreover maximum productivity is non-monotonic, peaking around the predicted value of $\hat{\lambda}$ (54) (dashed vertical line). In uncorrelated and anticorrelated environments, the best inactive timescale diverges ($\hat{\lambda} \rightarrow \infty$) and no peak is observed. As predicted for all three cases (Fig. 3a,b,c), when λ is

large, \mathcal{P}_0 is achieved by the bias given in (55). At low values of λ , the system has little time to re-balance during inactivity, and there is not enough time to erase the memory of previous active states. This hinders average productivity in the cases of uncorrelated and anticorrelated environments.

In Fig. 3a, the difference of maximum productivity at the best inactive timescale $\hat{\lambda}$ versus $\lambda \rightarrow \infty$ recovers the gap between the two bounds $\mathcal{P} - \mathcal{P}_0 = \Omega I_\pi(R; E_-)$. After normalization, this corresponds exactly to the mutual information between R and E_- . Recall that, in our example, $R \equiv E$, thus $I_\pi(R; E_-) = I_\pi(E; E_-) \approx 0.25$ (nats) is the mutual information between consecutive environment states. Hence, for positively correlated environments, the system can increase productivity by exploiting side information. When side information is erased ($\hat{\lambda} \rightarrow \infty$), the system can only achieve the no side-information bound, \mathcal{P}_0 . The gap between the overall productivity peak and the $\lambda \rightarrow \infty$ productivity (shown in green in Fig. 3a) quantifies the amount of information about the environment that the system uses to maximize productivity. This gap can serve as an empirical signature of functional information in this chemical system.

In the uncorrelated case of Fig. 3b, there is no mutual information between consecutive environments, thus no possibility of using side information. In the anticorrelated case Fig. 3c, correlations exist and can be encoded as side information (at finite λ), but this side information cannot be exploited by any achievable strategy to increase productivity. Thus, productivity never exceeds the no side-information bound \mathcal{P}_0 .

Finally, note that \mathcal{P} and \mathcal{P}_0 are not constant with respect to λ . This is because these bounds include the constant γ , which depends on λ through the total replicator concentration at the end of the inactive phase, the $X_{\emptyset|E_-}(\lambda)$ term in Eq. (51). At small λ , this concentration is close to $X_{\varepsilon_-}^*$, the steady-state concentration at the end of the previous active environment. We may plug this into (51) (and use that the two marginals of $p_{\varepsilon, \varepsilon_-}$ are equal) to show that $\gamma \approx 0$. Conversely, at long λ , the replicator concentration at the end of the inactive phase approaches $X_{\emptyset}^* \approx \mu > X_{\varepsilon}^*$ (since $k_f \gg k_d$). In this regime, $\gamma < 0$, which leads to an increase in productivity. This occurs because formation is favored over degradation, so most monomers assemble into replicators.

V. DISCUSSION

In this paper, we established a connection between information-theoretic measures and productivity in simple replicator systems exposed to fluctuating environments. In particular, we showed that productivity has information-theoretic contributions arising from environment uncertainty, side information, and the mismatch between the actual and optimal preparation strategies. We also derived the expression of the optimal strategy for maximizing productivity. We showed that the optimal strategy is biased toward slower-growing replicators. This kind of bias exemplifies the risk aversion exhibited when optimizing multiplicative growth, which in the well-known setting of Kelly gambling results in the proportional betting strategy [46]. Our approach extends existing ideas on

informational limits on growth and selection to the realistic setting of chemical and biological replicators in flow reactors.

To illustrate our theoretical findings, we explored a realistic model of photocatalytic replicators in a fluctuating environment [43]. We demonstrated that this autonomous system can implement a strategy, and that it can maintain an internal memory of previous environments that serves as a source of side information, without requiring additional sensing mechanisms. Finally, we showed that productivity can provide a signature of information flow in a plausible experimental setup. This analysis offers a new venue for understanding how chemical systems can exhibit information-processing in fluctuating conditions, and provides a simple example of memory in prebiotic self-replicators.

Our analysis of the photocatalytic replicators showed that productivity depends both on the replication rates of the replicators as well as the (slower) exchange reactions that lead to re-balancing of replicator concentrations. The information-theoretic contributions to productivity reflect the efficacy of the ‘information processing’ performed by the network, in terms of the alignment between environmental statistics and the implemented strategy. In certain prebiotic scenarios, one may consider productivity as the fitness of a replicator network, in which case networks may undergo selection for improved information processing. A possible realization may be provided by hydrothermal pore systems [63], conceptualized as a large number of small flow reactors for which different replicator networks compete. In such scenarios, although the contribution from information-theoretic terms to productivity may not be very large (only a few percent in Fig. 3a), the effect on resulting prebiotic evolution may be significant.

We mention several interesting directions for future research. First, our analysis of the photocatalytic replicator network was limited to first-order internal memory, where only the previous environment was tracked. Future work may consider networks that maintain higher-order memories, allowing for more complex environmental histories. Second, here we evaluated productivity for various fixed strategies. It is interesting to consider how simple systems may autonomously optimize their strategy, e.g., by modifying some slow internal variables [64]. Third, we considered purely deterministic chemical systems, assuming thermal fluctuations can be ignored. Extending our formalism to stochastic chemical reactions may shed light on how noise influences the relationship between information and productivity. Finally, it may be interesting to integrate our approach with recent results from nonequilibrium thermodynamics, as this may uncover novel relationship between thermodynamics and functional information in replicator systems.

ACKNOWLEDGMENTS

This project was supported by Grant No. 62417 from the John Templeton Foundation. The opinions expressed in this publication are those of the authors and do not necessarily reflect the views of the John Templeton Foundation.

AK was partly supported by the European Union's Horizon

2020 research and innovation programme under the Marie Skłodowska-Curie Grant Agreement No. 101068029.

-
- [1] A. Kolchinsky and D. H. Wolpert, "Semantic information, autonomous agency and non-equilibrium statistical physics," *Interface focus*, vol. 8, no. 6, p. 20180041, 2018.
- [2] D. R. Sowinski, J. Carroll-Nellenback, R. N. Markwick, J. Piñero, M. Gleiser, A. Kolchinsky, G. Ghoshal, and A. Frank, "Semantic information in a model of resource gathering agents," *PRX Life*, vol. 1, no. 2, p. 023003, 2023.
- [3] B. Ruzzante, L. Del Moro, M. Magarini, and P. Stano, "Synthetic cells extract semantic information from their environment," *IEEE Transactions on Molecular, Biological, and Multi-Scale Communications*, vol. 9, no. 1, pp. 23–27, 2023.
- [4] P. Godfrey-Smith and K. Sterelny, "Biological information," *Stanford Encyclopedia of Philosophy*, 2007.
- [5] D. R. Sowinski, A. Frank, and G. Ghoshal, "Information-theoretic description of a feedback-control kuramoto model," *Physical Review Research*, vol. 6, no. 4, p. 043188, 2024.
- [6] D. R. Sowinski, G. Ghoshal, and A. Frank, "Exo-Daisy World: Revisiting Gaia Theory through an Informational Architecture Perspective," *arXiv e-prints*, p. arXiv:2411.03421, Nov. 2024.
- [7] C. L. Nehaniv, D. Polani, K. Dautenhahn, R. te Boekhorst, and L. Canamero, "Meaningful information, sensor evolution, and the temporal horizon of embodied organisms," in *Artificial life VIII*, pp. 345–349, MIT Press Cambridge, MA, 2002.
- [8] E. V. Koonin, "The meaning of biological information," *Philosophical Transactions of the Royal Society A: Mathematical, Physical and Engineering Sciences*, vol. 374, no. 2063, p. 20150065, 2016.
- [9] J. Collier, "Information in biological systems," *Handbook of philosophy of science*, vol. 8, pp. 763–787, 2008.
- [10] R. M. Hazen, P. L. Griffin, J. M. Carothers, and J. W. Szostak, "Functional information and the emergence of biocomplexity," *Proceedings of the National Academy of Sciences*, vol. 104, no. suppl_1, pp. 8574–8581, 2007.
- [11] C. Adami, "What is complexity?," *BioEssays*, vol. 24, no. 12, pp. 1085–1094, 2002.
- [12] Y. Tu, "Quantitative modeling of bacterial chemotaxis: signal amplification and accurate adaptation," *Annual review of biophysics*, vol. 42, no. 1, pp. 337–359, 2013.
- [13] S. E. Palmer, O. Marre, M. J. Berry, and W. Bialek, "Predictive information in a sensory population," *Proceedings of the National Academy of Sciences*, vol. 112, no. 22, pp. 6908–6913, 2015.
- [14] G. Tkačik and W. Bialek, "Information processing in living systems," *Annual Review of Condensed Matter Physics*, vol. 7, no. 1, pp. 89–117, 2016.
- [15] H. H. Mattingly, K. Kamino, B. B. Machta, and T. Emonet, "Escherichia coli chemotaxis is information limited," *Nature physics*, vol. 17, no. 12, pp. 1426–1431, 2021.
- [16] M. Egbert, M. M. Hanczyc, I. Harvey, N. Virgo, E. C. Parke, T. Froese, H. Sayama, A. S. Penn, and S. Bartlett, "Behaviour and the origin of organisms," *Origins of Life and Evolution of Biospheres*, pp. 1–26, 2023.
- [17] E. Szathmáry and J. M. Smith, "The major evolutionary transitions," *Nature*, vol. 374, no. 6519, pp. 227–232, 1995.
- [18] C. Jeancolas, C. Malaterre, and P. Nghe, "Thresholds in origin of life scenarios," *Science*, vol. 23, no. 11, 2020.
- [19] M. Eigen, "Selforganization of matter and the evolution of biological macromolecules," *Naturwissenschaften*, vol. 58, pp. 465–523, 1971.
- [20] P. Schuster and K. Sigmund, "Replicator dynamics," *Journal of theoretical biology*, vol. 100, no. 3, pp. 533–538, 1983.
- [21] Y. Iwasa, "Free fitness that always increases in evolution," *Journal of Theoretical Biology*, vol. 135, no. 3, pp. 265–281, 1988.
- [22] G. von Kiedrowski, "Minimal replicator theory i: Parabolic versus exponential growth," *Bioorganic chemistry frontiers*, pp. 113–146, 1993.
- [23] G. P. Karev, "Replicator equations and the principle of minimal production of information," *Bulletin of mathematical biology*, vol. 72, pp. 1124–1142, 2010.
- [24] D. A. Baum, Z. Peng, E. Smith, A. M. Plum, and P. Gagrani, "The ecology–evolution continuum and the origin of life," *Journal of the Royal Society Interface*, vol. 20, no. 208, p. 20230346, 2023.
- [25] A. Kolchinsky, "Thermodynamics of darwinian evolution in molecular replicators," *arXiv preprint arXiv:2112.02809v4*, 2024.
- [26] A. Despons, Y. De Decker, and D. Lacoste, "Structural constraints limit the regime of optimal flux in autocatalytic reaction networks," *Communications Physics*, vol. 7, no. 1, p. 224, 2024.
- [27] G. von Kiedrowski, "A self-replicating hexadeoxynucleotide," *Angewandte Chemie International Edition in English*, vol. 25, no. 10, pp. 932–935, 1986.
- [28] D. H. Lee, J. R. Granja, J. A. Martinez, K. Severin, and M. R. Ghadiri, "A self-replicating peptide," *Nature*, vol. 382, no. 6591, pp. 525–528, 1996.
- [29] T. A. Lincoln and G. F. Joyce, "Self-sustained replication of an rna enzyme," *Science*, vol. 323, no. 5918, pp. 1229–1232, 2009.
- [30] P. T. Corbett, J. Leclaire, L. Vial, K. R. West, J.-L. Wieter, J. K. Sanders, and S. Otto, "Dynamic combinatorial chemistry," *Chemical reviews*, vol. 106, no. 9, pp. 3652–3711, 2006.
- [31] P. Adamski, M. Eleveld, A. Sood, Á. Kun, A. Szilágyi, T. Czárán, E. Szathmáry, and S. Otto, "From self-replication to replicator systems en route to de novo life," *Nature Reviews Chemistry*, vol. 4, no. 8, pp. 386–403, 2020.
- [32] S. Vela-Gallego, Z. Pardo-Botero, C. Moya, and A. de la Escosura, "Collective adaptability in a replication network of minimal nucleobase sequences," *Chemical Science*, vol. 13, no. 36, pp. 10715–10724, 2022.
- [33] A. K. Bandela, N. Wagner, H. Sadihov, S. Morales-Reina, A. Chotera-Ouda, K. Basu, R. Cohen-Luria, A. de la Escosura, and G. Ashkenasy, "Primitive selection of the fittest emerging through functional synergy in nucleopeptide networks," *Proceedings of the National Academy of Sciences*, vol. 118, no. 9, p. e2015285118, 2021.
- [34] R. Mizuuchi, T. Furubayashi, and N. Ichihashi, "Evolutionary transition from a single rna replicator to a multiple replicator network," *Nature Communications*, vol. 13, no. 1, p. 1460, 2022.
- [35] B. Damer and D. Deamer, "The hot spring hypothesis for an origin of life," *Astrobiology*, vol. 20, no. 4, pp. 429–452, 2020.
- [36] A. Ianeselli, A. Salditt, C. Mast, B. Ercolano, C. L. Kufner, B. Scheu, and D. Braun, "Physical non-equilibria for prebiotic nucleic acid chemistry," *Nature Reviews Physics*, vol. 5, no. 3, pp. 185–195, 2023.
- [37] G. Stephanopoulos, A. Frederickson, and R. Aris, "The growth

- of competing microbial populations in a cstr with periodically varying inputs,” *AIChE Journal*, vol. 25, no. 5, pp. 863–872, 1979.
- [38] S.-B. Hsu, “A competition model for a seasonally fluctuating nutrient,” *Journal of Mathematical Biology*, vol. 9, pp. 115–132, 1980.
- [39] J. M. Cushing, “Two species competition in a periodic environment,” *Journal of Mathematical Biology*, vol. 10, no. 4, pp. 385–400, 1980.
- [40] S. Pavlou, I. Kevrekidis, and G. Lyberatos, “On the coexistence of competing microbial species in a chemostat under cycling,” *Biotechnology and bioengineering*, vol. 35, no. 3, pp. 224–232, 1990.
- [41] H. L. Smith and P. E. Waltman, *The theory of the chemostat: dynamics of microbial competition*. No. 13 in Cambridge studies in mathematical biology, Cambridge ; New York, NY: Cambridge University Press, 1995.
- [42] C. E. Shannon, “A mathematical theory of communication,” *The Bell system technical journal*, vol. 27, no. 3, pp. 379–423, 1948.
- [43] K. Liu, A. Blokhuis, C. van Ewijk, A. Kiani, J. Wu, W. H. Roos, and S. Otto, “Light-driven eco-evolutionary dynamics in a synthetic replicator system,” *Nature Chemistry*, vol. 16, no. 1, pp. 79–88, 2024.
- [44] M. Kimura, “Natural selection as the process of accumulating genetic information in adaptive evolution,” *Genetics Research*, vol. 2, no. 1, pp. 127–140, 1961.
- [45] R. S. McGee, O. Kosterlitz, A. Kaznatcheev, B. Kerr, and C. T. Bergstrom, “The cost of information acquisition by natural selection,” *bioRxiv*, pp. 2022–07, 2022.
- [46] J. L. Kelly, “A new interpretation of information rate,” *The Bell System Technical Journal*, vol. 35, no. 4, pp. 917–926, 1956.
- [47] P. Haccou and Y. Iwasa, “Optimal mixed strategies in stochastic environments,” *Theoretical population biology*, vol. 47, no. 2, pp. 212–243, 1995.
- [48] E. Kussell and S. Leibler, “Phenotypic diversity, population growth, and information in fluctuating environments,” *Science*, vol. 309, no. 5743, pp. 2075–2078, 2005.
- [49] M. C. Donaldson-Matasci, C. T. Bergstrom, and M. Lachmann, “The fitness value of information,” *Oikos*, vol. 119, no. 2, pp. 219–230, 2010.
- [50] A. Mayer, T. Mora, O. Rivoire, and A. M. Walczak, “Transitions in optimal adaptive strategies for populations in fluctuating environments,” *Physical Review E*, vol. 96, no. 3, p. 032412, 2017.
- [51] J. R. Bernhardt, M. I. O’Connor, J. M. Sunday, and A. Gonzalez, “Life in fluctuating environments,” *Philosophical Transactions of the Royal Society B*, vol. 375, no. 1814, p. 20190454, 2020.
- [52] O. Rivoire and S. Leibler, “The value of information for populations in varying environments,” *Journal of Statistical Physics*, vol. 142, pp. 1124–1166, 2011.
- [53] A. S. Moffett and A. W. Eckford, “Minimal informational requirements for fitness,” *Physical Review E*, vol. 105, no. 1, p. 014403, 2022.
- [54] L. Dinis, J. Unterberger, and D. Lacoste, “Pareto-optimal trade-off for phenotypic switching of populations in a stochastic environment,” *Journal of Statistical Mechanics: Theory and Experiment*, vol. 2022, no. 5, p. 053503, 2022.
- [55] M. P. Robertson and G. F. Joyce, “Highly efficient self-replicating rna enzymes,” *Chemistry & biology*, vol. 21, no. 2, pp. 238–245, 2014.
- [56] I. Pepper, C. P. Gerba, T. Gentry, and R. M. Maier, *Environmental microbiology*. Academic press, 2009.
- [57] R. A. Armstrong and R. McGehee, “Competitive exclusion,” *The American Naturalist*, vol. 115, no. 2, pp. 151–170, 1980.
- [58] J. B. S. Haldane, “The cost of natural selection,” *Journal of Genetics*, vol. 55, pp. 511–524, 1957. Publisher: Springer.
- [59] W. Ewens, “Remarks on the substitutional load,” *Theoretical Population Biology*, vol. 1, pp. 129–139, Aug. 1970.
- [60] T. M. Cover, *Elements of information theory*. John Wiley & Sons, 1999.
- [61] G. Monreal Santiago, K. Liu, W. R. Browne, and S. Otto, “Emergence of light-driven protometabolism on recruitment of a photocatalytic cofactor by a self-replicator,” *Nature Chemistry*, vol. 12, no. 7, pp. 603–607, 2020.
- [62] J. A. Owen, A. Kolchinsky, and D. H. Wolpert, “Number of hidden states needed to physically implement a given conditional distribution,” *New Journal of Physics*, vol. 21, no. 1, p. 013022, 2019.
- [63] P. Baaske, F. M. Weinert, S. Duhr, K. H. Lemke, M. J. Russell, and D. Braun, “Extreme accumulation of nucleotides in simulated hydrothermal pore systems,” *Proceedings of the National Academy of Sciences*, vol. 104, no. 22, pp. 9346–9351, 2007.
- [64] S. Bartlett and D. Louapre, “Provenance of life: Chemical autonomous agents surviving through associative learning,” *Physical Review E*, vol. 106, no. 3, p. 034401, 2022.

APPENDICES

Appendix A: Derivation of main result, Eq. (28)

Using Eq. (25), we write

$$\langle \mathcal{P} \rangle = \langle \mathcal{P}^* \rangle + \frac{1}{\bar{\tau}} \sum_{\varepsilon, y} p_{\varepsilon, y} \frac{\phi_{\varepsilon}}{\eta_{r(\varepsilon)}} \left[\ln q_{r(\varepsilon)|y} + \ln \frac{X(0|y)}{X_{\varepsilon}^*} \right] \quad (\text{A1})$$

Using the definitions (31)-(32), which give the re-weighted probability distribution π over winning replicator and preparation variables R and Y . We combine and rewrite (A1) as

$$\langle \mathcal{P} \rangle = \langle \mathcal{P}^* \rangle - \gamma + \Omega \left[\sum_{r, y} \pi_{r, y} \ln q_{r|y} \right], \quad (\text{A2})$$

where γ uses definition (29). The remaining term between the brackets in (A2), which is multiplied by Ω , corresponds to minus an information-theoretic cost,

$$C_{\pi, q}(R|Y) := - \sum_{r, y} \pi_{r, y} \ln q_{r|y} \geq 0. \quad (\text{A3})$$

To show that this term indeed coincides with the second term appearing in (A1), it is easier to work backwards. We substitute definitions (31)-(32) into (A3):

$$\begin{aligned} C_{\pi, q}(R|Y) &= - \frac{1}{\Omega \bar{\tau}} \sum_{r, y} \sum_{\varepsilon: r(\varepsilon)=r} p_{\varepsilon, y} \frac{\phi_{\varepsilon}}{\eta_{r(\varepsilon)}} \ln q_{r|y} \\ &= - \frac{1}{\Omega \bar{\tau}} \sum_y \sum_{\varepsilon} \sum_r \delta_{r, r(\varepsilon)} p_{\varepsilon, y} \frac{\phi_{\varepsilon}}{\eta_{r(\varepsilon)}} \ln q_{r|y} \\ &= - \frac{1}{\Omega \bar{\tau}} \sum_{\varepsilon, y} p_{\varepsilon, y} \frac{\phi_{\varepsilon}}{\eta_{r(\varepsilon)}} \ln q_{r(\varepsilon)|y}, \end{aligned}$$

where in the second line we introduced the Kronecker delta $\delta_{r, r(\varepsilon)}$ to pick up on the winning replicator for environment ε and shifted the order of summation. Afterward, we multiply by $-\Omega$ and substitute terms to arrive at (28).

Appendix B: Photocatalytic replicator model

1. Active phase

During active phases, the system evolves according to:

$$\frac{da_\varepsilon}{dt} = (\mu - a_\varepsilon)\phi - (\eta_{1,\varepsilon}x_{1,\varepsilon} + \eta_{2,\varepsilon}x_{2,\varepsilon})a_\varepsilon + k_dX_\varepsilon - k_f a_\varepsilon, \quad (\text{B1})$$

$$\frac{dx_{1,\varepsilon}}{dt} = (\eta_{1,\varepsilon}a_\varepsilon - \phi)x_{1,\varepsilon} + k_f b a_\varepsilon - k_d x_{1,\varepsilon}, \quad (\text{B2})$$

$$\frac{dx_{2,\varepsilon}}{dt} = (\eta_{2,\varepsilon}a_\varepsilon - \phi)x_{2,\varepsilon} + k_f(1-b)a_\varepsilon - k_d x_{2,\varepsilon}, \quad (\text{B3})$$

Recall that we prepare the system such that $S(0) = S^* = \mu$ (for example, by letting the system flow at ϕ before starting the experiment). Hence, at all times we have that

$$S = a_\varepsilon + x_{1,\varepsilon} + x_{2,\varepsilon} = a_\varepsilon + X_\varepsilon = \mu. \quad (\text{B4})$$

In our setup, initial conditions for an active phase are given by the final concentration values from the previous inactive state, which we discuss next. We solve equations (B1), (B2) and (B3) numerically using the Runge-Kutta method. As an example, Fig. A1a shows the computed trajectories for $x_{1,\varepsilon}(t)$ and $x_{2,\varepsilon}(t)$ under weak light, $\varepsilon = \varepsilon'$.

2. Inactive phase

During inactive phases, the system evolves according to:

$$\frac{da_\emptyset}{dt} = k_d X_\emptyset - k_f a_\emptyset, \quad (\text{B5})$$

$$\frac{dx_{1,\emptyset}}{dt} = k_f b a_\emptyset - k_d x_{1,\emptyset}, \quad (\text{B6})$$

$$\frac{dx_{2,\emptyset}}{dt} = k_f(1-b)a_\emptyset - k_d x_{2,\emptyset}, \quad (\text{B7})$$

Using the constant solute concentration $S^* = \mu = a_\emptyset + X_\emptyset$,

$$\frac{dX_\emptyset}{dt} = k_f \mu - (k_d + k_f) X_\emptyset. \quad (\text{B8})$$

Given a previous environment $\varepsilon_- \in \{\varepsilon', \varepsilon''\}$, this gives the dynamics of the total replicator concentration, $X(t)$, during the inactive phase as

$$X_\emptyset(t|\varepsilon_-) = X_{\varepsilon_-}^* e^{-(k_f+k_d)t} + X_\emptyset^*(1 - e^{-(k_f+k_d)t}) \quad (\text{B9})$$

where we used definitions:

$$X_{\varepsilon'}^* := x_{1,\varepsilon'}^* + x_{2,\varepsilon'}^* \quad \text{and} \quad X_\emptyset^* := k_f \mu / (k_f + k_d). \quad (\text{B10})$$

Note that solution (B9) assumes that the preceding active phase has reached steady-state. We now solve for $\{x_{1,\emptyset}(t), x_{2,\emptyset}(t)\}$ by substituting back into (B6)-(B7) and applying initial conditions, which yields

$$x_{1,\emptyset}(t|\varepsilon_-) = \left[x_{1,\varepsilon_-}^* - \Delta_{1,\varepsilon_-}(t) \right] e^{-k_d t} + x_{1,\emptyset}^* (1 - e^{-k_d t}) \quad (\text{B11})$$

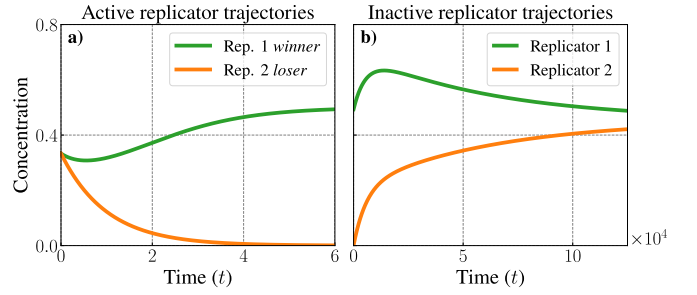


Figure A1. **Concentration trajectories.** For the same set of parameters as in Fig. 2: (a) shows the concentration trajectories during an active phase with $\varepsilon = \varepsilon'$ following Appendix B 1 with $a(0) = x_1(0) = x_2(0) = \mu/3$. (b) shows the inactive phase proceeding from the endpoints of the trajectories in the left panel by following Appendix B 2. The timescale difference between the subplots reflects the dominant rates in each phase.

$$x_{2,\emptyset}(t|\varepsilon_-) = \left[x_{2,\varepsilon_-}^* - \Delta_{2,\varepsilon_-}(t) \right] e^{-k_d t} + x_{2,\emptyset}^* (1 - e^{-k_d t}) \quad (\text{B12})$$

where we defined

$$\Delta_{1,\varepsilon}(t) := b(X_\varepsilon^* - X_\emptyset^*) (1 - e^{-k_f t}), \quad (\text{B13})$$

$$\Delta_{2,\varepsilon}(t) := (1-b)(X_\varepsilon^* - X_\emptyset^*) (1 - e^{-k_f t}), \quad (\text{B14})$$

and where we used definitions

$$x_{1,\emptyset}^* := bX_\emptyset^* \quad \text{and} \quad x_{2,\emptyset}^* := (1-b)X_\emptyset^*. \quad (\text{B15})$$

Fig. A1b shows trajectories (B11)-(B12) for $\varepsilon_- = \varepsilon'$. We note that the terms $e^{-k_d t}$ in (B11)-(B12) act as trade-off coefficients between the initial (square brackets) and steady-state inactive phase concentrations. Note that, at the end of the inactive phase $t = \tau_I$, $e^{-k_d t}|_{t=\tau_I} = e^{-\lambda}$, hence the dimensionless inactive timescale $\lambda = k_d \tau_I$ controls this trade-off.

Finally, we define the concentrations at the end of an inactive phase as functions of $\{b, \lambda\}$, and conditioned on the state of the previous active phase by substituting for $t = \tau_I$ in (B11) and (B12). If we assume that the active steady states are approximately $x_{1,\varepsilon'}^* \approx x_{2,\varepsilon'}^* \approx 0$, then the final concentrations at inactive phases are approximated as

$$x_{1,\emptyset}^{\varepsilon''}(b, \lambda) \approx b \left[X_{\emptyset|\varepsilon''}(\lambda) - x_{2,\varepsilon''}^* e^{-\lambda} \right], \quad (\text{B16})$$

$$x_{2,\emptyset}^{\varepsilon'}(b, \lambda) \approx (1-b) \left[X_{\emptyset|\varepsilon'}(\lambda) - x_{1,\varepsilon'}^* e^{-\lambda} \right]. \quad (\text{B17})$$

Here we defined $x_{i,\emptyset}^{\varepsilon_-}(b, \lambda) := x_{i,\emptyset}(\tau_I|\varepsilon_-)$ for $i = 1, 2$ as the replicator concentrations at the end of an inactive phase preceded by light intensity ε_- . By substituting of $t = \tau_I$ in (B9), we use $X_{\emptyset|\varepsilon_-}(\lambda) := X_\emptyset(\tau_I|\varepsilon_-)$ for the total concentration, which depends on λ but not on b .

3. Conditions on p and π in correlated vs. anticorrelated environments

This appendix contains three results. First, we show that

$$p_{\varepsilon',\varepsilon'} - p_{\varepsilon'} p_{\varepsilon'}' = p_{\varepsilon'',\varepsilon''} - p_{\varepsilon''} p_{\varepsilon''}' \quad (\text{B18})$$

where $p_{\varepsilon, \varepsilon_-} = p_{\varepsilon_-} p_{\varepsilon|\varepsilon_-}$ and $p'_\varepsilon = \sum_{\varepsilon_-} p_{\varepsilon, \varepsilon_-}$. To do so, we write the left hand side of (B18) as

$$(1 - p_{\varepsilon'} - p'_{\varepsilon'} + p_{\varepsilon', \varepsilon'}) - (1 - p_{\varepsilon'}) (1 - p'_{\varepsilon'}) \quad (\text{B19})$$

then simplify to arrive at the right hand side. In our case, p is the steady-state distribution, so $p = p'$ leads to Eq. (43).

Second, assuming p has full support, we show that

$$p_{\varepsilon', \varepsilon'} - p_{\varepsilon'}^2 > 0 \quad \implies p_{\varepsilon'|\varepsilon'} > p_{\varepsilon'} \quad (\text{B20})$$

$$\implies p_{\varepsilon', \varepsilon'} - p_{\varepsilon'}^2 > 0 \quad \implies p_{\varepsilon', \varepsilon'} > p_{\varepsilon'}. \quad (\text{B21})$$

The second line follows from (B18), the last implication in each line follows by dividing both sides by $p_{\varepsilon'}$ and $p_{\varepsilon', \varepsilon'}$ respectively. Adding gives

$$p_{\varepsilon', \varepsilon'} - p_{\varepsilon'}^2 > 0 \quad \implies p_{\varepsilon'|\varepsilon'} + p_{\varepsilon', \varepsilon'} > 1. \quad (\text{B22})$$

The same kind of derivation gives the converse,

$$p_{\varepsilon', \varepsilon'} - p_{\varepsilon'}^2 \leq 0 \quad \implies p_{\varepsilon'|\varepsilon'} + p_{\varepsilon', \varepsilon'} \leq 1. \quad (\text{B23})$$

Lastly, we show the equivalence between statements:

$$p_{\varepsilon'|\varepsilon'} + p_{\varepsilon', \varepsilon'} > 1 \iff \pi_{1|\varepsilon'} + \pi_{2|\varepsilon'} < 1, \quad (\text{B24})$$

and $p_{\varepsilon'|\varepsilon'} + p_{\varepsilon', \varepsilon'} = 1$ being equivalent to $\pi_{1|\varepsilon'} + \pi_{2|\varepsilon'} = 1$. As shown below in Appendix B 4, condition (B24) also guarantees the existence of a finite optimal timescale $\hat{\lambda}$. We begin by studying

$$\begin{aligned} \pi_{1|\varepsilon'} + \pi_{2|\varepsilon'} &= \frac{\pi_{1, \varepsilon'}}{\pi_{1, \varepsilon'} + \pi_{2, \varepsilon'}} + \frac{\pi_{2, \varepsilon'}}{\pi_{1, \varepsilon'} + \pi_{2, \varepsilon'}} \\ &= \frac{p_{\varepsilon', \varepsilon'}}{p_{\varepsilon', \varepsilon'} + p_{\varepsilon', \varepsilon'}} + \frac{p_{\varepsilon', \varepsilon'}}{p_{\varepsilon', \varepsilon'} + p_{\varepsilon', \varepsilon'}}, \quad (\text{B25}) \end{aligned}$$

where, in the last line, we used definitions in (52)-(53). For convenience, we parametrize the conditional distribution $p_{\varepsilon|\varepsilon_-}$ as

$$\begin{aligned} p_{\varepsilon'|\varepsilon'} &= \frac{\Gamma + \Delta}{2}, & p_{\varepsilon'|\varepsilon'} &= 1 - \frac{\Gamma - \Delta}{2}, \\ p_{\varepsilon', \varepsilon'} &= 1 - \frac{\Gamma + \Delta}{2}, & p_{\varepsilon', \varepsilon'} &= \frac{\Gamma - \Delta}{2}. \end{aligned} \quad (\text{B26})$$

In this parametrization, we note that $\Gamma = p_{\varepsilon'|\varepsilon'} + p_{\varepsilon', \varepsilon'}$ quantifies the conditional probabilities of staying in the same active state ($\varepsilon|\varepsilon_-$), while $\Delta = p_{\varepsilon'|\varepsilon'} - p_{\varepsilon', \varepsilon'}$ quantifies the difference of staying probability in weak versus strong active states. Next, the marginal probability for weak light state is given by:

$$p_{\varepsilon'} = p_{\varepsilon'|\varepsilon'} p_{\varepsilon'} + p_{\varepsilon', \varepsilon'} (1 - p_{\varepsilon'}), \quad (\text{B27})$$

which is solved as

$$p_{\varepsilon'} = \frac{1 + \frac{\Gamma - \Delta}{2}}{2 - \Gamma} \quad \text{and} \quad p_{\varepsilon'} = 1 - p_{\varepsilon'}. \quad (\text{B28})$$

Combining our parametrization (B26) and (B28), using $p_{\varepsilon, \varepsilon_-} = p_{\varepsilon|\varepsilon_-} p_{\varepsilon_-}$ and plugging into (B25) gives

$$\pi_{1|\varepsilon'} + \pi_{2|\varepsilon'} = 1 + \frac{1 - \Gamma}{\Pi}. \quad (\text{B29})$$

with $\Pi := \left[\frac{\Gamma - \Delta}{2} + \frac{\eta_2}{\eta_1} \left(1 - \frac{\Gamma - \Delta}{2} \right) \right] \left[\frac{\Gamma + \Delta}{2} + \frac{\eta_1}{\eta_2} \left(1 - \frac{\Gamma + \Delta}{2} \right) \right]$. Note that the second term in (B29) vanishes when $\Gamma = 1$. Hence, $\Gamma = p_{\varepsilon'|\varepsilon'} + p_{\varepsilon', \varepsilon'} = 1$ implies $\pi_{1|\varepsilon'} + \pi_{2|\varepsilon'} = 1$.

Furthermore, if in (B29) we take derivatives of $\pi_{1|\varepsilon'} + \pi_{2|\varepsilon'}$ with respect to Γ , we obtain

$$-\frac{1}{2} \left[\left(\frac{\eta_2}{\eta_1} \right) \left(\frac{\Gamma - \Delta}{2} + \frac{\eta_2}{\eta_1} \left(1 - \frac{\Gamma - \Delta}{2} \right) \right)^{-2} + \left(\frac{\eta_1}{\eta_2} \right) \left(\frac{\Gamma + \Delta}{2} + \frac{\eta_1}{\eta_2} \left(1 - \frac{\Gamma + \Delta}{2} \right) \right)^{-2} \right],$$

which is strictly negative as long as $\eta_1, \eta_2 > 0$. This observation implies that $\pi_{1|\varepsilon'} + \pi_{2|\varepsilon'}$ is strictly decreasing in Γ for any fixed Δ . Therefore, this proves (B24).

4. Best achievable strategy

In order to study the best achievable strategy, we recall from our main result, Eq. (28), that all the dependence on the strategy q is encoded in our information-theoretic cost $C_{\pi, q}(R|Y)$, given in Eq. (34).

In our example introduced in Sec. IV, the parameters that control q are $\{b, \lambda\}$, i.e., $q = q(b, \lambda)$. In general, there may not be values of $\{b, \lambda\}$ such that q equals π and thus achieves maximum productivity. However, we can still optimize the contribution in (34) in each case.

Let us write the strategy conditional on the previous environment states as fractions of respective concentrations evaluated at the end of the inactive phase:

$$q_{1|\varepsilon'}(b, \lambda) \approx \frac{x_{1, \emptyset}^{\varepsilon'}(b, \lambda)}{X_{\emptyset|\varepsilon'}(\lambda)} = \left[1 - \frac{x_{1, \emptyset}^* e^{-\lambda}}{X_{\emptyset|\varepsilon'}(\lambda)} \right] b, \quad (\text{B30})$$

$$q_{2|\varepsilon'}(b, \lambda) \approx \frac{x_{2, \emptyset}^{\varepsilon'}(b, \lambda)}{X_{\emptyset|\varepsilon'}(\lambda)} = \left[1 - \frac{x_{1, \emptyset}^* e^{-\lambda}}{X_{\emptyset|\varepsilon'}(\lambda)} \right] (1 - b), \quad (\text{B31})$$

with $q_{2|\varepsilon'} = 1 - q_{1|\varepsilon'}$ and $q_{1|\varepsilon'} = 1 - q_{2|\varepsilon'}$, where we used Eq. (B16) and Eq. (B17).

We approximate the expressions for $q_{r|\varepsilon_-}$ by assuming that formation is favored over degradation, $k_f \gg k_d$ and that $\tau_I k_f \gg 1$. These assumptions guarantee that $X_{\emptyset|\varepsilon_-}(\lambda) \approx \mu$ for $\varepsilon_- = \varepsilon', \varepsilon', \varepsilon'$, see Eqs. (B8) and (B10). Using the estimate for steady-state replicator concentration values, $x_{1, \varepsilon'}^* \approx \mu - \phi/\eta_1$ and $x_{2, \varepsilon'}^* \approx \mu - \phi/\eta_2$, we arrive at the following approximation for the strategy as a function of control parameters:

$$q_{1|\varepsilon'}(b, \lambda) \approx \left[1 - \left(1 - \frac{\phi}{\eta_2 \mu} \right) e^{-\lambda} \right] b, \quad (\text{B32})$$

$$q_{2|\varepsilon'}(b, \lambda) \approx \left[1 - \left(1 - \frac{\phi}{\eta_1 \mu} \right) e^{-\lambda} \right] (1 - b), \quad (\text{B33})$$

Further simplification is obtained by assuming that $\eta_1, \eta_2 \gg \phi/\mu$, such that we ignore the terms like $\phi/\eta_i \mu$ inside brackets,

$$q_{1|\varepsilon'}(b, \lambda) \approx (1 - e^{-\lambda}) b, \quad (\text{B34})$$

$$q_{2|\mathcal{I}}(b, \lambda) \approx (1 - e^{-\lambda})(1 - b). \quad (\text{B35})$$

Next, we use the expressions above to solve for the best achievable strategy. As mentioned in the main text, the best strategy is given by minimizing $C_{\pi,q}(R|Y)$ (30) with respect to the bias b and dimensionless inactive timescale λ . First, we approximate cross-entropy term as a function of $\{b, \lambda\}$ by plugging in approximations (B34)-(B35) into (30) and using conditional distribution $\pi_{R|Y}$, which yields

$$\begin{aligned} C_{\pi,q}(R|Y) &\approx -\pi_{1|\mathcal{I}}\pi_{\mathcal{I}} \ln [1 - (1 - e^{-\lambda})(1 - b)] \\ &\quad - \pi_{1|\mathcal{I}'}\pi_{\mathcal{I}'} \ln [(1 - e^{-\lambda})b] \\ &\quad - \pi_{2|\mathcal{I}}\pi_{\mathcal{I}} \ln [(1 - e^{-\lambda})(1 - b)] \\ &\quad - \pi_{2|\mathcal{I}'}\pi_{\mathcal{I}'} \ln [1 - (1 - e^{-\lambda})b]. \end{aligned} \quad (\text{B36})$$

Next, we use $\pi_{1|\mathcal{I}} = 1 - \pi_{1|\mathcal{I}'}$, $\pi_{2|\mathcal{I}'} = 1 - \pi_{2|\mathcal{I}}$, and $\pi_{\mathcal{I}'} + \pi_{\mathcal{I}} = 1$. We find the optimal bias and dimensionless timescale are obtained by taking derivatives and equating to zero as

$$\partial_b C_{\pi,q}(R|Y)|_{b=\hat{b}} = 0, \quad \partial_\lambda C_{\pi,q}(R|Y)|_{\lambda=\hat{\lambda}} = 0.$$

With a bit of algebra (or software like Mathematica), this

system of equations can be solved to give

$$\hat{b} \approx \frac{\pi_{1|\mathcal{I}'}}{\pi_{1|\mathcal{I}'} + \pi_{2|\mathcal{I}'}} \quad \text{and} \quad \hat{\lambda} \approx -\ln(1 - \pi_{1|\mathcal{I}'} - \pi_{2|\mathcal{I}'}).$$

This solution is not valid for uncorrelated and anticorrelated systems, for which $\pi_{1|\mathcal{I}'} + \pi_{2|\mathcal{I}'} \geq 1$, because the critical point is outside of the valid parameter region $(b, \lambda) \in [0, 1] \times \mathbb{R}^+$. Therefore, for uncorrelated and anticorrelated systems, the minimum of $C_{\pi,q}(R|Y)$ must either be achieved on the boundaries ($b = 0$ or $b = 1$ and $\lambda = 0$), or not achieved so that $C_{\pi,q}(R|Y)$ continually decreases as $\lambda \rightarrow \infty$. However, from (B36), we note that, for $b \rightarrow 0$, $b \rightarrow 1$, and $\lambda \rightarrow 0$, $C_{\pi,q}(R|Y) \rightarrow +\infty$ due to the $\ln(0)$ terms. Hence, the minimum cannot be achieved in the boundaries, which means that the best timescale for uncorrelated and anticorrelated environments diverges,

$$\lambda \rightarrow \infty. \quad (\text{B37})$$

Moreover, by studying $\lim_{\lambda \rightarrow \infty} C_{\pi,q}(R|Y)$ as a function of b , and maximizing, gives:

$$\hat{b}_{\lambda \rightarrow \infty} = \pi_{1|\mathcal{I}'} + \pi_{1|\mathcal{I}} = \pi_1. \quad (\text{B38})$$